

This is a repository copy of *An ab initio approach to the Hugoniot*.

White Rose Research Online URL for this paper:

<https://eprints.whiterose.ac.uk/218354/>

Version: Published Version

Article:

Wilkins, Jacob and Probert, Matt orcid.org/0000-0002-1130-9316 (2024) An ab initio approach to the Hugoniot. *The Journal of Chemical Physics*. 144113. ISSN 1089-7690

<https://doi.org/10.1063/5.0229565>

Reuse

This article is distributed under the terms of the Creative Commons Attribution (CC BY) licence. This licence allows you to distribute, remix, tweak, and build upon the work, even commercially, as long as you credit the authors for the original work. More information and the full terms of the licence here:

<https://creativecommons.org/licenses/>

Takedown

If you consider content in White Rose Research Online to be in breach of UK law, please notify us by emailing eprints@whiterose.ac.uk including the URL of the record and the reason for the withdrawal request.

RESEARCH ARTICLE | OCTOBER 10 2024

An *ab initio* approach to the Hugoniot

Jacob S. Wilkins ; Matt I. J. Probert  



J. Chem. Phys. 161, 144113 (2024)

<https://doi.org/10.1063/5.0229565>



Articles You May Be Interested In

Uniaxial Hugoniot: Method and Applications

AIP Conference Proceedings (July 2002)

Shock-induced transformations in crystalline RDX: A uniaxial constant-stress Hugoniot molecular dynamics simulation study

J. Chem. Phys. (July 2009)

Density functional tight binding calculations for the simulation of shocked nitromethane with LATTE-LAMMPS

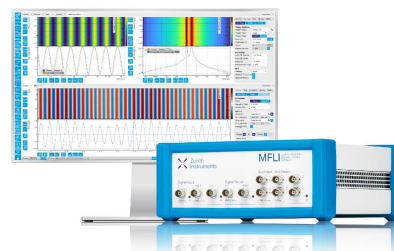
AIP Conference Proceedings (July 2018)

Challenge us.

What are your needs for periodic signal detection?



[Find out more](#)



An *ab initio* approach to the Hugoniot

Cite as: J. Chem. Phys. 161, 144113 (2024); doi: 10.1063/5.0229565

Submitted: 18 July 2024 • Accepted: 25 September 2024 •

Published Online: 10 October 2024



View Online



Export Citation



CrossMark

Jacob S. Wilkins^{1,2}  and Matt I. J. Probert^{1,a)} 

AFFILIATIONS

¹School of Physics, Engineering and Technology, University of York, York YO10 5DD, United Kingdom

²Scientific Computing Department, STFC Rutherford Appleton Laboratory, Didcot OX11 0QX, United Kingdom

^{a)}Author to whom correspondence should be addressed: matt.probert@york.ac.uk

ABSTRACT

The Hugoniot is the equation of state of a shock-compressed material and is a key part of high-pressure physics. One way of calculating it is via the Hugoniotstat that has significant computational advantages over direct calculation via non-equilibrium molecular dynamics. We introduce a number of improvements to the Hugoniotstat, which significantly reduce the run time and the number of atoms required for converged results. Consequently, *ab initio* Hugoniot calculations are tractable. We illustrate the benefits through simple model potentials and with density functional theory calculations of argon.

© 2024 Author(s). All article content, except where otherwise noted, is licensed under a Creative Commons Attribution (CC BY) license (<https://creativecommons.org/licenses/by/4.0/>). <https://doi.org/10.1063/5.0229565>

I. INTRODUCTION

High-pressure physics is a fascinating area of study, posing significant challenges to both experiment and theory. It is also an area of practical significance, from materials development in engineering to extreme geophysical studies.¹ For instance, recently, there has been a lot of controversy in high-pressure studies (both theoretical and experimental) about potential room-temperature superconductors.²

High-pressure physics experiments have two main ways of reaching extreme conditions: either static (diamond anvil cell or other compression) or dynamic (shock waves). Unfortunately, although many developments in recent years have greatly improved the levels of accuracy and time scales that are accessible to experiments, many of the processes that we would wish to measure in real materials remain inaccessible due to time scale, or simply the material or the experimental apparatus required to measure them is prohibitively expensive. This is where the power of computer simulation can step in and relieve the burden. While static calculations make it simple to simulate states of high pressure, these are often also at zero temperature and, hence, unrepresentative of experiments. Hence, the majority of such calculations are dynamic, to incorporate both high pressure and temperature.

All molecular dynamics (MD) calculations that use periodic boundary conditions can suffer from significant finite-size effects. Direct non-equilibrium molecular dynamics (NEMD) calculations

of shock waves³ have been developed for some time; however, because of the need to propagate a shock wave, they require a large number of atoms to be simulated. Hence, these have traditionally used simple model potentials for the inter-atomic interactions to manage the computational cost. The limitation of this approach is the accuracy of the potentials, which either require empirical data or high-quality *ab initio* calculations on small systems, to parameterize the potential(s). The shock front can also generate highly disordered states, which may be very short-lived transients, further complicating the generation of a model potential. The obvious solution to these issues is a full *ab initio* molecular dynamics (AIMD) calculation of the shocked state; however, this has, until now, been too computationally expensive (except for a few “hero calculations,” e.g., see Ref. 4) for routine application. One approach to accelerating *ab initio* calculations is to use a classical force field to generate a set of configurations, sample the independent configurations using a more expensive *ab initio* method, and then reweight the samples.⁵ This has been used with Monte Carlo successfully but has many complications with MD calculations. There have also been recent developments in the merging of machine-learning approaches “on the fly” with *ab initio* molecular dynamics,⁶ but this has yet to be attempted with shock-wave states. For a recent review of shock wave simulations, see Ref. 7.

The set of (T,P) states reachable by any shock wave is given by the solution of the Rankine–Hugoniot^{8,9} equations, which is often known as the “Hugoniot.” In this paper, we will show how an exist-

ing molecular dynamics approach to the calculation of states on the Hugoniot—known as the Hugoniot¹⁰—can be extended and improved so that it is now practical to use with an *ab initio* approach. An alternative equilibrium shock simulation technique, which has been developed since the Hugoniot approach, is the multiscale shock technique (MSST).¹¹ This has the advantage that it can simulate multiple shocks and allows access to the dynamics of the shock wave while requiring fewer atoms than the NEMD approach. However, it requires iteration over an estimate of the shock velocity to reach a consistent state and a “cell mass” hyperparameter that can affect the structural evolution. A recent comparative study¹² found that, for liquid methane, the traditional Hugoniot approach generated a slightly more accurate Hugoniot curve but was 3× slower than the MSST approach. As will be shown, our modified Hugoniot is free from hyperparameter tuning, requires no iteration, is ergodic, and is significantly more computationally efficient than before. We will validate our new approach to the Hugoniot using classical pair potential calculations with the reference Hugoniot implementation in the LAMMPS code¹³ and compare it to our new implementation in the CASTEP code.¹⁴ We will then use this new approach to perform a full *ab initio* calculation of the Hugoniot of argon and compare the results to the experimental data.

II. THEORY

A. The Hugoniot equation of state

During early developments in the study of discontinuities and their stability and presence in fluids, Rankine⁸ and Hugoniot⁹ independently discovered some key relationships via the conservation laws of fluids. These were found by Rayleigh¹⁵ to be the same solutions from different perspectives, and thus, this system of equations is now called the Rankine–Hugoniot equations. The state of the system determined by these equations is referred to as the “Hugoniot.”

The Hugoniot equations describe the locus of all possible thermodynamic states reachable by the shocked system, and so form the basis for the equation of state of a shock wave and describe how a shock wave discontinuity forms on both sides of the shock front. It is formed from three fundamental conservation laws for mass, momentum, and energy,

$$\rho_1 u_1 = \rho_2 u_2, \quad (1)$$

$$\rho u_1^2 + P_1 = \rho u_2^2 + P_2, \quad (2)$$

$$h_1 + \frac{1}{2} u_1^2 = h_2 + \frac{1}{2} u_2^2, \quad (3)$$

where subscripts 1 and 2 refer to the state of the system ahead of and behind the shock-front, respectively; ρ is the mass density of the fluid; u is the fluid velocity; P is the pressure; and h is the specific enthalpy (per unit mass). It can also be formulated in terms of the shock speed,

$$\rho_1 u_s = \rho_2 (u_s - u_2), \quad (4)$$

$$P_2 - P_1 = \rho_2 u_2 (u_s - u_2) = \rho_1 u_s u_2, \quad (5)$$

$$P_2 u_2 = \rho_1 u_s \left(\frac{1}{2} u_2^2 + e_2 - e_1 \right), \quad (6)$$

where u_s is the shock speed and e is the specific internal energy. Using substitutions of Eqs. (4) and (5) into Eq. (6), it is possible to derive the Hugoniot equation,

$$e_2 - e_1 = \frac{1}{2} (P_1 + P_2) (\rho_1^{-1} - \rho_2^{-1}), \quad (7)$$

which on the per-unit-mass basis gives us

$$e_2 - e_1 = \frac{1}{2} (P_1 + P_2) (V_1 - V_2). \quad (8)$$

Finally, for many materials, the shock (u_s) and particle (u_p) velocities are related by a linear dependence,¹⁶

$$u_s = v_s + s u_p, \quad (9)$$

where v_s is the speed of sound and s is some material-dependent constant.

The shock and particle velocities are direct observables in an NEMD calculation, but they can also be extracted from a Hugoniot via

$$u_s = \sqrt{\frac{P - P_0}{\rho_0 (1 - \varepsilon)}}, \quad (10)$$

$$u_p = \sqrt{\frac{(P - P_0)(1 - \varepsilon)}{\rho_0}}, \quad (11)$$

$$= u_s (1 - \varepsilon), \quad (12)$$

and hence, this can be used to test Eq. (9).

B. Hugoniotats

1. Nosé–Hoover

The uniaxial Hugoniot (NVHug) was created by Maillet *et al.*¹⁰ and is a constant volume approach to the calculation of the Hugoniot. It uses a Nosé–Hoover style of integrator to drive the temperature of the system to the state on the Hugoniot corresponding to the given compression.

Using the conventional symbols for particle position \vec{r}_i , momentum \vec{p}_i , mass m_i , and force \vec{F}_i , the equations of motion for the Nosé–Hoover NVHug method are

$$\dot{\vec{r}}_i = \frac{\vec{p}_i}{m_i}, \quad (13)$$

$$\dot{\vec{p}}_i = \vec{F}_i - \nu \chi \vec{p}_i, \quad (14)$$

$$\dot{\chi} = \frac{\nu}{C} (E(t) - E_H(t)), \quad (15)$$

where χ is the heat flow of the thermostat into the system, ν is the coupling between the thermostat and the system, C is a scaling constant in units of energy to conserve system size independence, and

$$E_H(t) = E(t_0) + \frac{1}{2}(P(t) + P(t_0))(V(t_0) - V(t)), \quad (16)$$

where t_0 is the time before the system has been compressed (i.e., the equilibrium state). The instantaneous energy of the system is given by $E(t)$ and the deviation of the current state from the Hugoniot state is the Hugoniot estimator, $E(t) - E_H(t)$.

The uniaxial Hugonostat as given has an instantaneous compression to the shocked volume, followed by a thermal relaxation to the Hugoniot state. This can cause significant transients and so it was later suggested by Maillet that a steady compression should be used instead. This idea was then taken further by adding a barostat, resulting in a variable cell approach, giving rise to the NPHug formulation.¹⁷ While this approach is very useful for simulations using model potentials, it is significantly less efficient for *ab initio* calculations using a plane-wave basis set as this depends on the size and/or shape of the simulation cell. CASTEP uses a plane-wave basis and so we do not explore variable cell methods such as NPHug or MSST further here.

2. Langevin

The Langevin thermostat¹⁸ is a thermostat based on the idea of the system containing a gas of fictitious particles held at a fixed temperature, colliding with the sample material, as in Brownian motion. It can be shown that this thermostat is both ergodic and symplectic,¹⁹ which is not the case with the standard Nosé–Hoover thermostat. A scheme for a Langevin-based Hugonostat was given in Ref. 20 using temperature as a dynamical variable and building a dynamical sampling of the configuration space from previous exploration of the system by the trajectory. This is done by creating a histogram of the expectation value of the Hugoniot estimator at given temperature distributions and, thus, attempting to drive the temperature to that of the correct expectation value for the Hugoniot. This formulation is complex to implement and inefficient in practice.

III. METHOD

We shall first describe the various improvements we have made to the standard Hugonostat formulations, with a focus on *ab initio* implementations. We have implemented the Nosé–Hoover NVHug method in CASTEP as a reference to test and validate against.

A. Langevin Hugonostat

The NVHug Langevin formulation alluded to in Ref. 20 was not stated in a form that could be implemented using instantaneous system properties. We have derived a means of calculating a Langevin integrator following the same scheme as the Langevin integrator already present in CASTEP, although the temperature is replaced by a Hugoniot estimator [Eq. (19)]. The advantage of a Langevin thermostat is that it is guaranteed to be ergodic because of the Gaussian fluctuations.

The equations of motion that govern the new Langevin Hugonostat are

$$\dot{\vec{r}}_i = \frac{\vec{p}_i}{m_i}, \quad (17)$$

$$\dot{\vec{p}}_i = \vec{F}_i - \underbrace{\gamma \vec{p}_i}_{\text{Damping Term}} + \underbrace{\sqrt{\frac{2m_i k_B T \gamma}{\Delta t}} N(0, 1)}_{\text{Fluctuation}}, \quad (18)$$

$$\dot{T} = \frac{-vT_0}{C}(E(t) - E_H(t)), \quad (19)$$

where γ is a coupling constant that determines the decorrelation time of the system (i.e., the time over which the velocities of the particles may be considered no longer correlated), $N(0, 1)$ is a random number from the standard normal distribution, v determines the coupling of the Hugonostat to the heat bath, T_0 is the pre-shock temperature, Δt is the time step used, T is the temperature estimator, and C is the same scaling constant as in Eq. (15). C is in units of energy to conserve system size independence, and it was suggested in Maillet *et al.*¹⁰ that this should be the “unit of energy of the interaction potential.” As an analog in DFT simulations, we use

$$C = N\epsilon, \quad (20)$$

where N is the total number of atoms in the system and ϵ is the average chemical potential, and this seems to work well.

As a first validation that the new Langevin NVHug method converges to the same state point as the Nosé–Hoover NVHug method, we present a 500-atom Lennard-Jones simulation in Fig. 1 after a 30% compression. This shows that both methods converge to the same state point, but that the Langevin method does not exhibit the same initial transient “spike” seen in the temperature and pressure traces. While this is harmless for a Lennard-Jones simulation, such transients would be very detrimental in *ab initio* calculations, significantly increasing the cost of each AIMD step. The Langevin method also has less noise, suggesting that it would be better for sampling. However, this also shows the need to reduce the time to come to equilibrium.

The standard Nosé–Hoover thermostat has known issues with ergodicity and sensitivity to choice of coupling parameters. The Langevin approach followed here is one way to fix these issues. It was also shown in Ref. 19 how these issues can be fixed with their Nosé–Hoover–Langevin approach, thus that approach could also be used here.

In this work, we shall describe the application of the Langevin approach to the NVHug method. It can be trivially extended to the constant pressure NPHug method, following the same approach as in Ref. 21.

B. Extensions

In AIMD calculations, rapid changes in the structure can lead to poor DFT convergence and calculations can become unstable at high temperatures. Second, if atoms become very close, then the fundamental assumptions of pseudopotential-based calculations can break down. DFT is also very expensive to calculate compared to empirical force fields, thus the methods need to be as efficient as possible, for example, with minimal transients. We cannot afford to perform numerous DFT simulations as trial runs to find the best parameter values before formulating the final calculation. Hence, it is necessary to construct a methodology that is both robust and predictable from

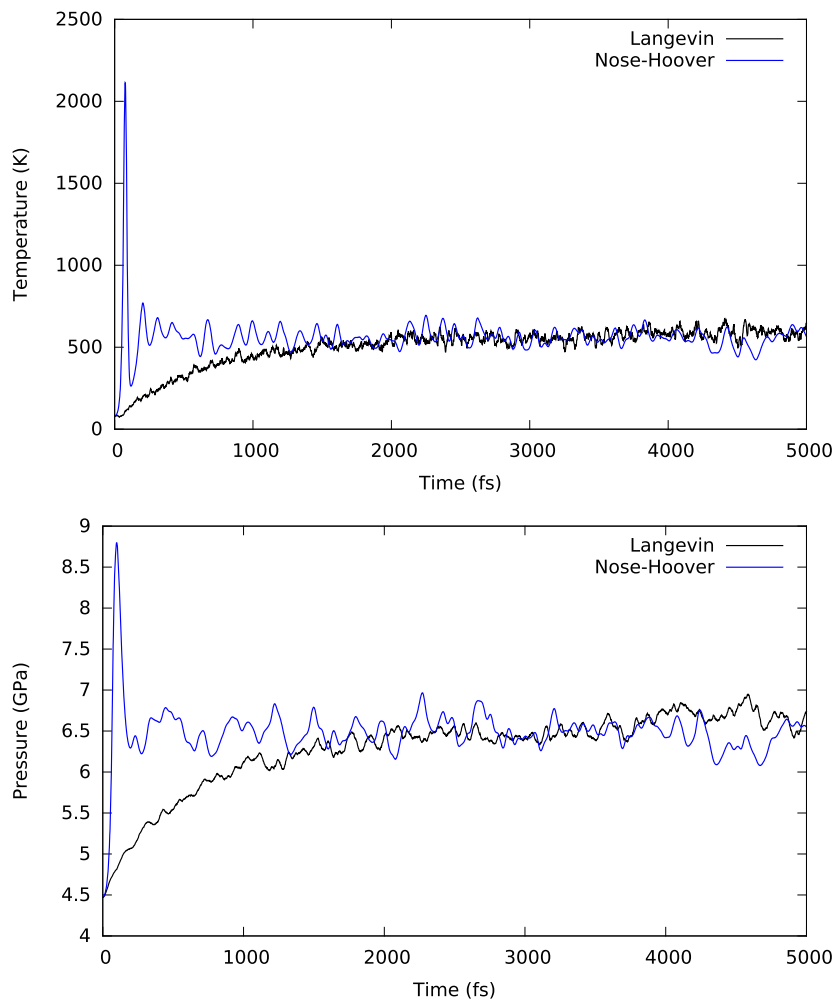


FIG. 1. A comparison of the convergence of the NVHug Nosé-Hoover and NVHug Langevin to the Hugoniot state for a 500-atom Lennard-Jones cell. Note the lack of a transient state in the Langevin formulation. Using more advanced damping and quenching techniques (Secs. III B 1 and III B 2), the convergence rate of both can be significantly increased and transients removed.

the outset. This is very difficult to achieve in a complex and variable system such as a shock wave.

We present here several of the modifications we have made to account for these problems in DFT calculations.

1. Damping

As was suggested in Ref. 17, it is possible to achieve a more rapid equilibration to the Hugoniot temperature by applying damping to the Nosé-Hoover formulation of the Hugoniotstat such that the equation for the update Eq. (15) becomes

$$\dot{\chi} = \frac{v}{C}(E(t) - E_H(t)) - \beta_{NH}\chi, \quad (21)$$

where χ is the heat flow and β_{NH} is a user-defined damping coefficient for the heat flow, chosen to bring about critical damping to

the Hugoniot state. This has been implemented into the CASTEP Nosé-Hoover NVHug.

The equivalent for the Langevin implementation is difficult to formulate since the equivalent of χ is the temperature, as discussed in Sec. III A, and that has an unknown target value. Instead, we modify the coupling factor during the equilibration phase if we detect that the rate of change of temperature has changed sign, meaning an oscillation around the ideal target value,

$$\text{if } \dot{T}^{n-1}\dot{T}^n < 0 \text{ then: } v \rightarrow (1 - \beta_L)v, \quad (22)$$

where superscript n refers to the time step. Note that we do not apply damping once the equilibration period is over.

This serves to slow the dynamics of the temperature and attempts to minimize the amount of overshoot while still leaving the system free to explore and modify the temperature. More

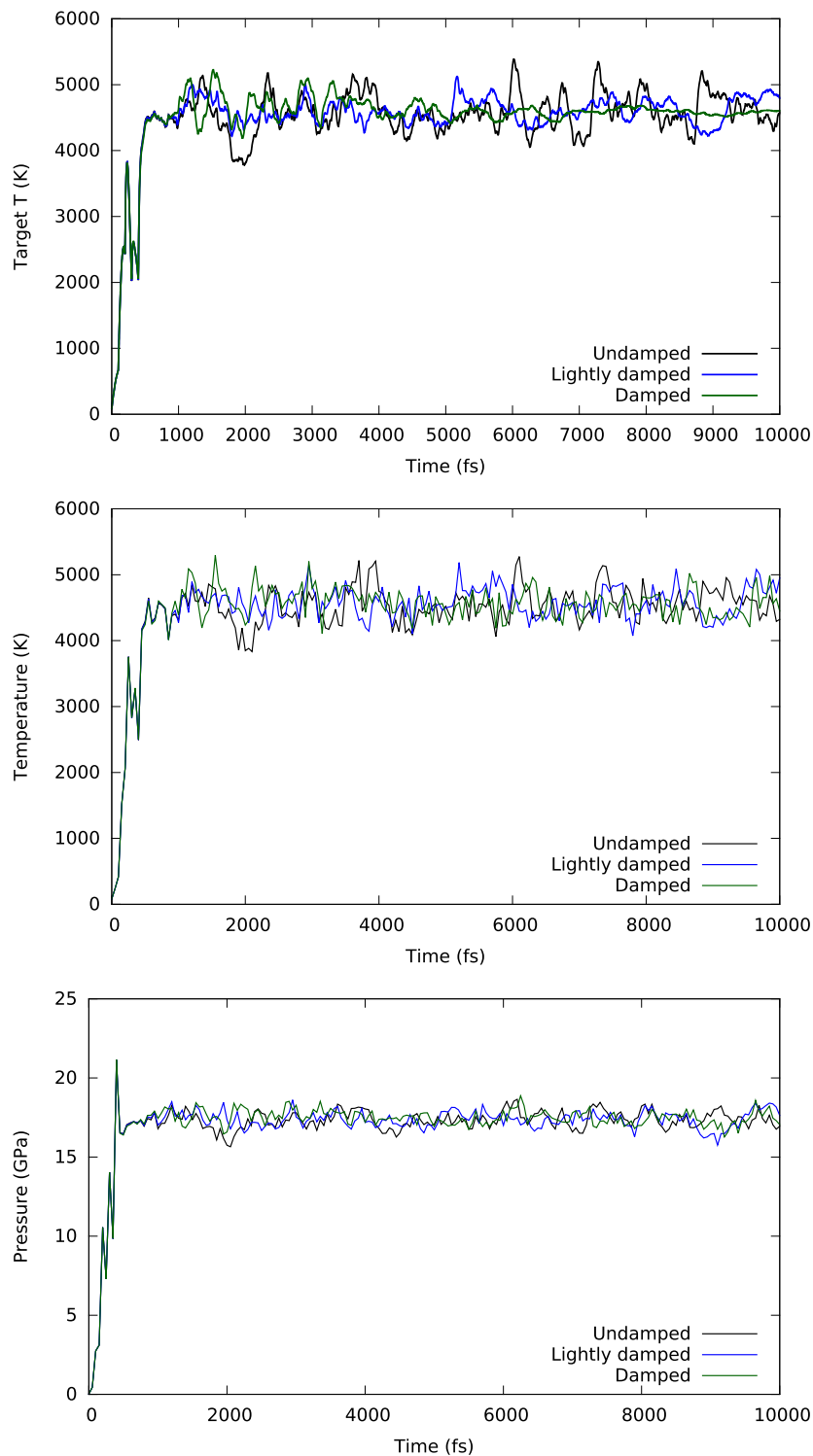


FIG. 2. Effects of the damping on the Langevin scheme for a 500-atom Lennard-Jones cell at a 60% compression with an overly strong Hugoniot coupling (ν) of 0.1 fs^{-1} and a damping factor (β_L) of (Undamped) 0.0, (Lightly Damped) 0.1, (Damped) 0.3. Top: Convergence of the target temperature to that of the Hugoniot temperature is accelerated and smoothed. Middle and Bottom: Convergence of the system properties, with a sample every 50 fs. Note that the mean of the system properties are effectively unchanged, but with lower variance.

advanced methods could be implemented to apply an adaptive step-size method to the dynamics; however, as an initial smoothing mechanism, this approach is found to be sufficient as seen in Fig. 2. This shows that a β_L of 0.3 with the Langevin NVHug scheme can significantly reduce initial overshoot at the expense of a slightly slower convergence to the final temperature.

2. Quenching

It is also possible to improve the equilibration time of the Nosé–Hoover Hugonostat using a similar rapid convergence technique from damped MD geometry optimization.²² A quenching scheme for the Hugonostat also helps to significantly reduce transient effects, see Fig. 3. If we consider the Nosé–Hoover Hugonostat variable (χ) as being like a velocity of the temperature (T) and the change in the Hugonostat variable ($\dot{\chi}$) as being like the acceleration, we can apply a quenching scheme in which

$$\text{if } \chi\dot{\chi} < 0 \text{ then: } \chi = 0. \quad (23)$$

This is permissible because the heat flow variable (χ) is not directly affecting the system but only modifying a fictitious variable, which, in turn, affects the dynamics of the system. This first-order separation from the simulation itself means that the system is still free to continue exploring configurations as it would if unquenched. This is also made more acceptable, given that the data from the transient/equilibration period is usually excluded from the calculation of equilibrium properties. Therefore, the optimal approach to quenching is to restrict it so that it is only active during a pre-specified equilibration time and the system acts under the pure Hugonostat after this time.

The same idea can also be applied to quenching the piston variable of the NPHug method, which consequently prevents large transient cell size/shape changes.

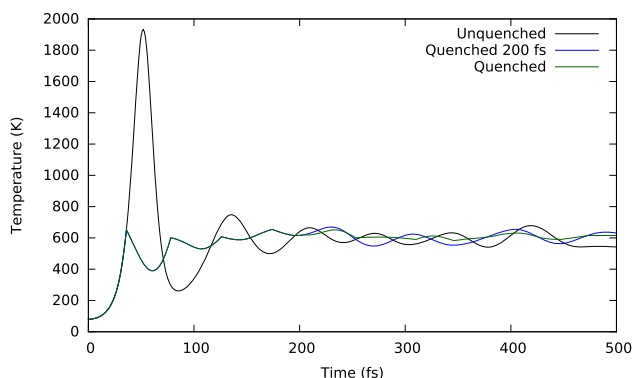


FIG. 3. The effects of quenching on the temperature of a 30% compressed 500-atom Lennard-Jones system, using the Nosé–Hoover NVHug method. The unquenched line (black) shows a large initial transient, while the quenched lines (blue and green) show the elimination of this transient at the expense of “unphysical” temperature dynamics, which are eliminated when the quenching is turned off (blue) after equilibration. It should be noted that all three converge to the same temperature.

3. Predictor

Previous applications of the Hugonostat method have generated one state point on the Hugoniot curve. With expensive DFT calculations, it is best to reuse as much information as possible from one state point calculation to the next, to minimize transients and equilibration time. Hence, we have developed a predictor algorithm to calculate a series of constant-volume Hugonostat runs with uniform sampling in the pressure space of the Hugoniot to construct the full Hugoniot in a fire-and-forget manner.

Given a target pressure and a number of desired steps, the predictor can automatically trace the Hugoniot curve to minimize the amount of effort needed from the user. It is capable of calculating a number of Hugoniot properties such as the coupling of the Nosé–Hoover Hugonostat and estimating the temperature, speed of sound, and speed of shock in the target system.

The algorithm and approaches used in this section are described in the Appendix.

Both linear and quadratic predictors were implemented because, until the quadratic predictor has sufficient information to function properly (an underdetermined equation), it uses a linear predictor. The linear predictor only uses the previous two data points, whereas the quadratic scheme can use a user-specified length of history. An example can be seen in Fig. 4, which shows the resulting Hugoniot for an 864-atom LJ test system, from a single run.

We have also built a fail-safe mechanism into the predictor, such that should there be a discontinuity in the Hugoniot (e.g., due to a phase transition); the predictor will forget its history and build forward from that point. This detection is a simple mechanism

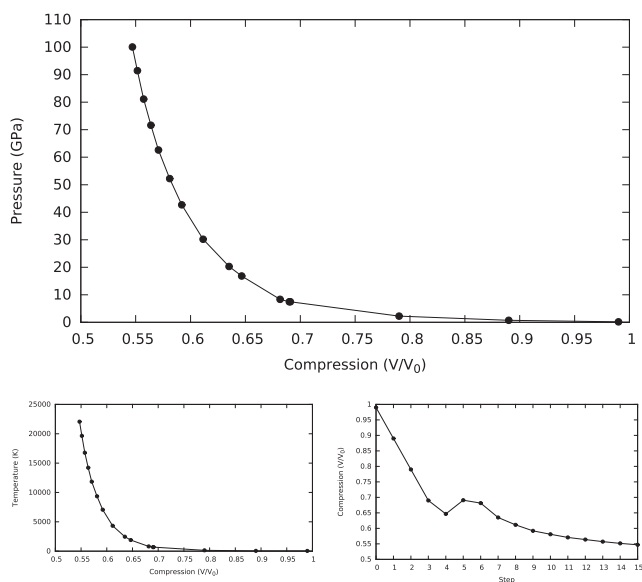


FIG. 4. Result of the Hugoniot predictor algorithm for an 864-atom Lennard-Jones cell using the Langevin integrator. Top: Compression against pressure. Bottom left: Temperature against pressure. Bottom right: Compression against predictor step. Calculations were performed using a second-order polynomial predictor aiming to step from 0 to 100 GPa in steps of 10 GPa, with a permitted error of 20% to the target.

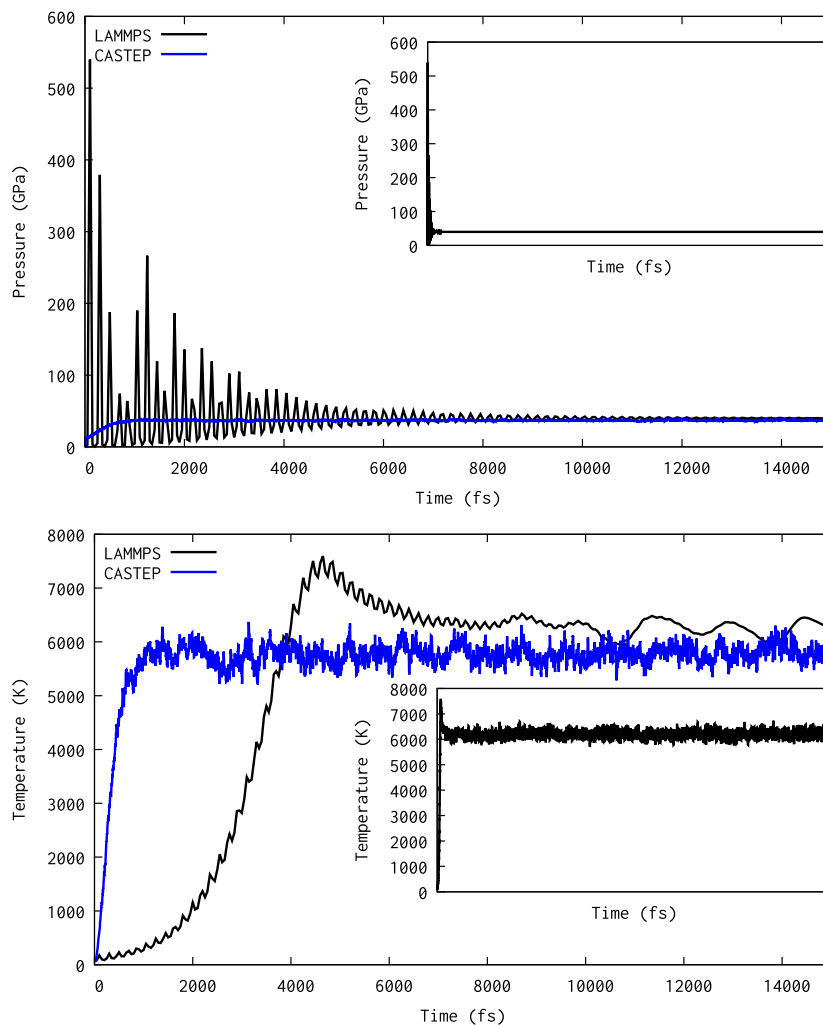


FIG. 5. Comparison of this work's implementation of the Hugoniot and a reference implementation in the LAMMPS code. The results of CASTEP are using an 864-atom Lennard-Jones perfect FCC cell and the Langevin NVHug method at 60% compression (~ 36 GPa). LAMMPS' results are those of a Nosé–Hoover NPHug on a 2048-atom Lennard-Jones FCC cell at 40 GPa. The inset graphs show the full trajectory of the 500 000 fs LAMMPS run to demonstrate its convergence.

that just ensures linearity such that as compression is increased, temperature and pressure increase correspondingly.

4. Coupling

The coupling ν depends on the compression. Consequently, if a single static value was used with the predictor, it would be impossible to simulate harder materials, as the calculations would soon become unstable as the compression increased. It was suggested in the original Nosé–Hoover Hugoniot paper¹⁰ that the coupling is related to the Einstein frequency (ω_E) of the material. The calculation of curvatures of potentials mid-calculation is expensive and not guaranteed to be accurate, especially for non-equilibrium states where the potential is likely to be very anharmonic. Instead, we propose a mechanism for estimating the related Debye frequency (ω_D), based on the derivative of the predictor function.

We know that

$$v_s = \sqrt{\frac{B}{\rho}}, \quad (24)$$

where v_s is the speed of sound, B is the bulk modulus ($V \frac{\partial^2 E}{\partial V^2}$), and ρ is the density ($\frac{N}{V}$). The predictor relates P and V (via ϵ) and allows us to take a trivial derivative of the predictor's fitted function, which gives us

$$\frac{\partial P}{\partial \epsilon} \approx v_s^2, \quad (25)$$

which can then be used with the usual formula for the Debye frequency,²³

$$\omega_D = v_s \sqrt{6\pi^2 \rho}. \quad (26)$$

We can initialize the coupling at ambient pressure using a reasonable guess at the bulk modulus B and then use Eq. (26) within the predictor to obtain a reasonable value for the next coupling based on the material in its current dynamic state.

IV. RESULTS

A. Lennard-Jones potential

The reference implementation for the Hugoniot is the Nosé–Hoover NPHug implementation in the LAMMPS code.¹³ To demonstrate the efficacy of our implementation, we first must verify that our results agree with the standard implementation.

The Lennard-Jones (LJ) potential²⁴ is one of the most common testing potentials used in molecular dynamics as it is very cheap and fast to calculate. The potential is designed to represent the van der Waals' interactions occurring in noble gases such as Argon.

The LJ potential is of the following form:

$$V_{LJ}(r_{ij}) = 4\epsilon \left(\left(\frac{\sigma}{r_{ij}} \right)^6 - \left(\frac{\sigma}{r_{ij}} \right)^{12} \right), \quad (27)$$

where r_{ij} is the separation of atoms i and j , ϵ controls the depth of the potential well, and σ controls the width of the potential well.

It is often parameterized to low-temperature argon, with $\epsilon = 120.0k_B$ and $\sigma = 3.405 \text{ \AA}$.

With the LAMMPS NPHug, it is possible to specify the pressure and the Hugoniot will find the corresponding state on the Hugoniot with the matching temperature. With our NVHug, it is the compression that is specified. A comparison is shown in Fig. 5, which shows the dramatically improved convergence and lack of transients in our implementation, and close agreement with the final state. From this, we estimate that the cumulative effect of our improvements is a ten-fold reduction in the run time required to achieve convergence compared to the original Hugoniot.

It is more useful to trace out the full Hugoniot. In LAMMPS, we can do this as a set of runs, each with a specified pressure. In CASTEP, we can do this with the predictor, aiming to reach 100 GPa in steps of ~ 10 GPa. The results can be seen in Fig. 6. Although there are slight deviations at high pressures/compressions, these deviations are well within expected fluctuations for any MD calculation, in which both temperature and pressure fluctuations scale as $N^{-\frac{1}{2}}$ for a system containing N atoms.

B. BKS quartz

A more complex test system is quartz. The BKS potential developed by van Beest *et al.*²⁵ was parameterized to a series of Hartree–Fock calculations to model clusters of aluminosilicophos-

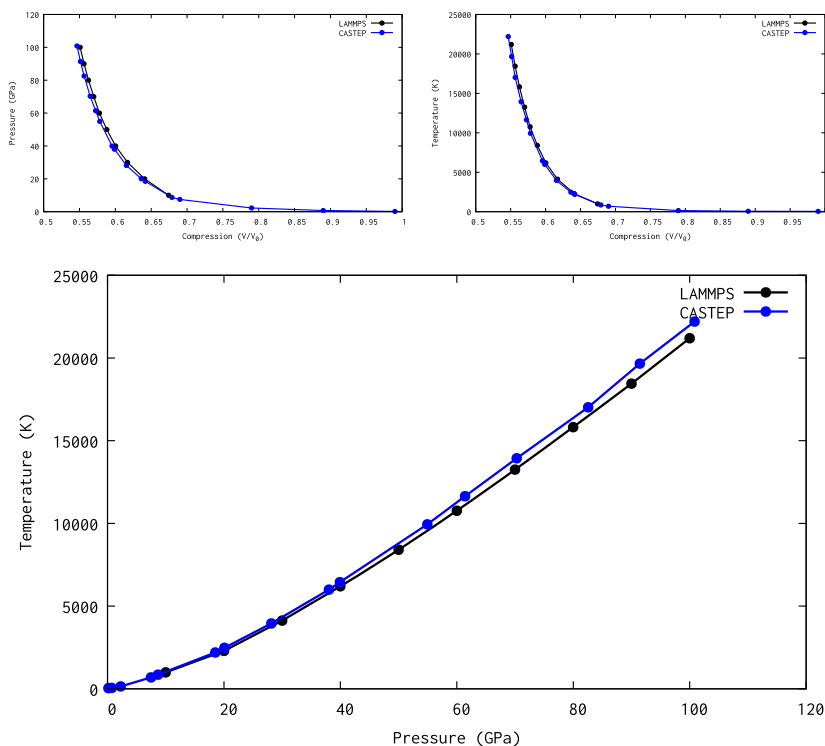


FIG. 6. Comparison of Hugoniot calculated using this work's implementation of the Hugoniot and a reference implementation in the LAMMPS code. The results of CASTEP are using an 864-atom Lennard-Jones perfect FCC cell and the Langevin NVHug linear predictor method, attempting to reach 100 GPa in steps of 10 GPa. LAMMPS' results are those of a series of Nosé–Hoover NPHug on a 2048-atom Lennard-Jones FCC cell, taking steps in pressure of 10 GPa.

TABLE I. BKS parameters from Ref. 25.

$\alpha\beta$	r_{cut} (Å)	A (eV)	b (Å ⁻¹)	C (eV Å ⁶)	q
Si–O	6.0	18 003.7572	4.873 18	133.5381	$q_{Si} = 2.4$
O–O	6.0	1388.773	2.76	175	$q_O = -1.2$

phases and has often been applied to quartz. They adopted the form of a Buckingham exponential²⁶ with an additional Coulomb term,

$$V_{BKS}(r_{ij}) = A_{\alpha\beta} \exp(-b_{\alpha\beta}r_{ij}) - \frac{C_{\alpha\beta}}{r_{ij}^6}, \quad (28)$$

$$V_{Coulomb}(r_{ij}) = \frac{q_{\alpha}q_{\beta}}{r_{ij}}, \quad (29)$$

where α and β are labels of the species of atoms i and j , respectively, and the BKS parameters are given in Table I.

These terms are combined,

$$V_{tot}(r_{ij}) = \begin{cases} V_{BKS}(r_{ij}) + V_{Coulomb}(r_{ij}), & r_{ij} < r_{cut}, \\ V_{Coulomb}(r_{ij}), & r_{ij} > r_{cut}, \end{cases} \quad (30)$$

and the Coulomb interaction is evaluated by Ewald's method to account for the long-range convergence issues and is applied at all r_{ij} .

The original form has issues with atom overlap at high pressure, and therefore, short-range corrections were proposed in Ref. 27 to fix this,

$$V_{sr}(r_{ij}) = \frac{D_{\alpha\beta}}{r_{ij}^2} + \frac{E_{\alpha\beta}}{r_{ij}^6} + F_{\alpha\beta}, \quad (31)$$

and so now

$$V_{tot}(r_{ij}) = \begin{cases} V_{sr}(r_{ij}) + V_{Coulomb}(r_{ij}), & r_{ij} < r_{sr}, \\ V_{BKS}(r_{ij}) + V_{Coulomb}(r_{ij}), & r_{sr} < r_{ij} < r_{cut}, \\ V_{Coulomb}(r_{ij}), & r_{ij} > r_{cut}. \end{cases} \quad (32)$$

The original parameters as defined in Ref. 27 were found to cause a discontinuity in the potential, leading to erroneous results. To correct this, a new set of parameters was derived for the correction in this work and are given in Table II.

Initial attempts to use the uniaxial Hugoniot on α -quartz resulted in an unphysical divergence in the target temperature to negative values. The origin of this issue is the anisotropic nature of α -quartz such that when compressed along the perpendicular axis

TABLE II. Short-range modifications to the BKS potential.

Source	$\alpha\beta$	r_{sr} (Å)	D (eV Å ²)	E (eV Å ⁶)	F (eV)
Ref. 27	Si–O	1.35	24.17	23.8086	-3.5872
	O–O	1.98	12.3435	18.9662	-6.9426
This work	Si–O	1.37	10.9219	20.5976	-6.437 63
	O–O	1.99	23.4731	27.4136	-3.467 79

(which we call Z), it disperses the pressure laterally along the x and y axes, which leads to a drop in the measured pressure in the direction of compression. Recall that, in the uniaxial Hugoniot–Rankine equation,

$$E_H = E_0 - \frac{1}{2}(P_{zz} + P_0)(V - V_0), \quad (33)$$

the only contributing stress component is that in the direction of compression. Hence, we modified this equation so that the compression for the NVHug CASTEP calculations was performed isotropically by applying

$$\mathbf{h}_{comp} = \epsilon \mathbf{I} \cdot \mathbf{h}_0, \quad (34)$$

where \mathbf{h} is the matrix of cell vectors for the structure and ϵ is the compression of the cell, defined as $\frac{V}{V_0}$. Hence, the Hugoniot–Rankine equation is replaced with

$$E_H = E_0 - \frac{1}{2} \left(\frac{1}{3} \text{Tr}(\mathbf{P}) + P_0 \right) (V - V_0). \quad (35)$$

We can now compare LAMMPS calculations using the uniaxial (along the C axis) constant-pressure Nosé–Hoover Hugoniot, with the new isotropic constant-volume Langevin Hugoniot predictor in CASTEP. The LAMMPS calculations used 576 atoms from 10 to 100 GPa in steps of 10 GPa but with extra measurements taken at 15 and 18 GPa to attempt to capture the collapse of the α -quartz structure. The CASTEP calculations were performed using either 72- or 576-atom α -quartz cells from 20 to 200 GPa in steps of ~20 GPa using the predictor method.

Figure 7 shows that both the LAMMPS and CASTEP Hugoniot calculations for BKS quartz show a strong reproduction of the trends displayed in the results obtained by Refs. 28 and 29 for α -quartz shocks in the higher pressure regions, although, at lower pressures, there is some discrepancy in the LAMMPS data. This could be explained by an early phase transition in the BKS potential³⁰ or due to the anisotropy of the quartz crystal, by the crystal direction in which the shocks are occurring. The CASTEP Hugoniot follows the lower compression trends much more closely, although there is a significant drop in the measured pressure around a compression of 0.63, which could be due to a phase transition in the

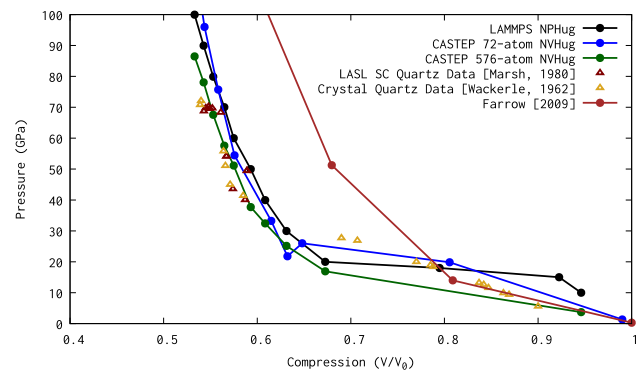


FIG. 7. Compression-pressure Hugoniot for BKS α -quartz with experimental data taken from Refs. 28 and 29 and theoretical data from Ref. 31.

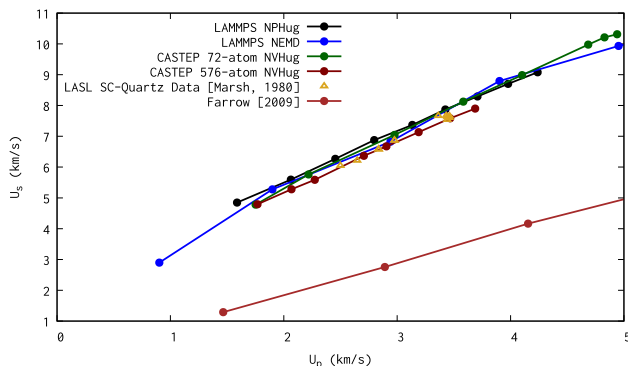


FIG. 8. Shock-particle velocity Hugoniot for BKS α -quartz with experimental data taken from Ref. 28 and theoretical data from Ref. 31.

TABLE III. Calculated Hugoniot slopes and speed of sound and corresponding standard errors of the fit for BKS shocks calculated by different methods. Experimental data from Ref. 28 are included.

Source	s	v_s (km/s)
CASTEP NVHug	1.73 ± 0.02	1.84 ± 0.09
LAMMPS NPHug	1.60 ± 0.02	2.34 ± 0.07
Ref 28	1.72 ± 0.06	1.72 ± 0.19

material or a secondary collapse of the α -quartz structure. The discontinuity in the Hugoniot around 10–20 GPa is likely due to a transition to a phase transition between the α -quartz phase and the stishovite phase, resulting in a volume drop.

Both the Hugoniot methods agree extremely well with the experiment for the u_s - u_p Hugoniot as shown in Fig. 8. The large disagreement with the results of Ref. 31 probably comes from the flaws in the short-range potential used there, which have been fixed in this work. The results of fitting the Hugoniot data to Eq. (9) are given in Table III and show that even though both Hugoniot methods use the same potential, the CASTEP results are significantly close to the experimental data.

Hence, these results show that the new isotropic constant-volume Langevin Hugoniot predictor can accurately generate a Hugoniot curve, including a structural phase transition, with a remarkably small number of atoms. Note the close agreement between 72- and 576-atom results shown in Fig. 8 and the experimental data.

C. DFT argon

The main focus of this paper is to make feasible the calculation of the Hugoniot for any material without significant prior parameterization, i.e., using *ab initio* methods. The many modifications we have made to the Hugoniot method have focused on optimizing the approach for DFT calculations in a static cell (NVHug) simulation.

To demonstrate the performance with DFT, we present calculations using CASTEP on 108-atom cells of argon. This system is small

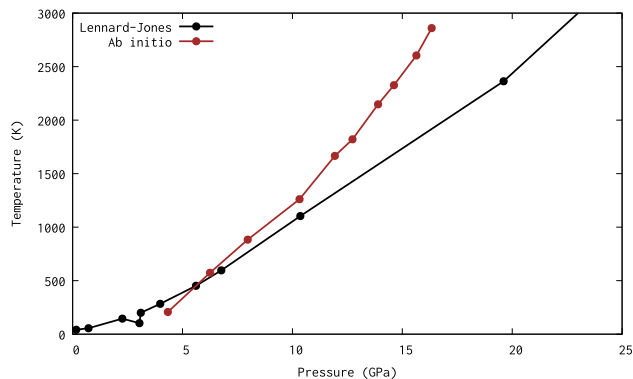


FIG. 9. Pressure-temperature Hugoniot plot comparing 864-atom Lennard-Jones perfect FCC cell and 108-atom DFT argon perfect FCC cell using Langevin NVHug.

enough to be easily tractable with DFT, and as such may have finite size errors, but the results in Sec. IV B show that this system size is probably sufficient to get reasonable results. The DFT calculations used the PBE exchange-correlation functional and a standard norm-conserving pseudopotential. The plane-wave cut-off energy was set to 550 eV, and the Brillouin-zone sampling was chosen to be 0.05 \AA^{-1} to give reasonable accuracy without damaging performance.

Figure 9 shows the Hugoniot extracted from the DFT calculations of argon. The discrepancy between the DFT and the LJ calculations is believed to be primarily due to the fundamental differences between LJ and DFT argon, rather than finite-size effects. As the Lennard-Jones potential is parameterized for low temperature, ambient pressure argon, and fixed during the Hugoniot calculation, we would expect deviations to occur as the system is put under extreme conditions, whereas the DFT calculation can adapt.

Figure 10 shows the corresponding u_s - u_p curve for the LJ and DFT data, and experimental data of Ref. 32. The DFT data, despite small system size, aligns surprisingly well with the experimental data,

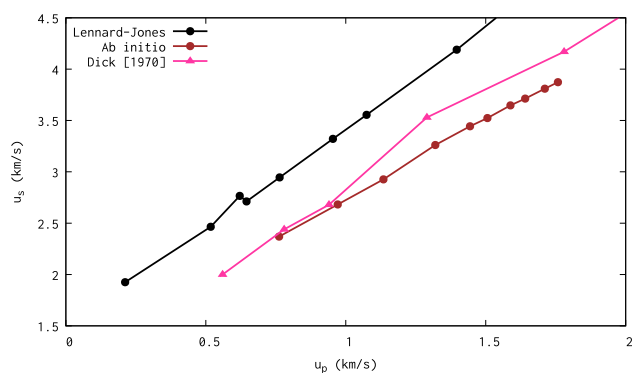


FIG. 10. Shock-Particle velocity Hugoniot of argon comparing 864-atom Lennard-Jones perfect FCC cell and 108-atom DFT argon perfect FCC cell using Langevin NPHug, experimental data taken from Ref. 32.

TABLE IV. Calculated Hugoniot slopes and speed of sound and corresponding standard errors of the fit for Argon shocks calculated by different methods. Experimental data for the speed of sound in solid Argon is included from Refs. 32 and 33.

Source	s	v_s (km/s)
Lennard-Jones	1.92 ± 0.01	1.55 ± 0.04
DFT	1.53 ± 0.02	1.21 ± 0.03
Ref. 32	1.62 ± 0.04	1.29 ± 0.11
Ref. 33	...	1.26–1.35

and the agreement is significantly better than for the LJ data. This can also be seen quantitatively in Table IV. This shows the benefit of an *ab initio* approach over a fitted potential, with transferability to arbitrary pressure and temperature regimes.

V. CONCLUSION

We have demonstrated that *ab initio* calculation of the Hugoniot of a material is now a reasonable computational endeavor, without requiring excessive supercomputer resources. We have

ALGORITHM 1. Hugoniot predictor algorithm, with fail-safe, reuse, and Nosé–Hoover coupling sections. \leftarrow implies push on the front of the array (unshift). `take_predictor_step` is described in Algorithm 2.

Input: Cell state at t_{final} , history

Output: New cell state

if initializing **then**

 history $\leftarrow [1, P_0, T_0, E_0]$

 save backup of original cell

 compression initialized to some small value

if restart **then**

 history $\leftarrow [\varepsilon, P, T, E]$ {Read all old history}

end if

end if

calculate average P, T and E of previous predictor step

history $\leftarrow [\varepsilon, P_{av}, T_{av}, E_{av}]$

print $[\varepsilon, P_{av}, T_{av}, E_{av}]$

if $|P_{av} - P_{target}| < \Delta P$ **then**

$i =$ steps taken {Check prior history to avoid repeats}

while $i > 0$ **do**

if $|\text{history}[i][P] - P_{target}| < \Delta P$ **then**

$P_{target} += P_{step}$

$i =$ steps taken

end if

$i = i - 1$

end while

end if

$\varepsilon, \text{deriv} = \text{take_predictor_step}(P_{target}, \text{history}, V_0, \varepsilon)$

if $\varepsilon < 0$ **or** $\varepsilon > 1$ **then**

abort Instability in predictor

end if

if reuse **and** $\text{history}^1[\varepsilon] > \varepsilon$ **then**

Continue

else

 reset cell to initial state

end if

compress cell to new volume and re-initialize MD variables

if Nosé–Hoover **then**

$v_s = \sqrt{\text{deriv}/V_0}$

$\text{tmpcoup} = v_s^3 \sqrt{6\pi^2 \rho}$

$\text{coup} = \max(\text{coup}, \text{tmpcoup})$ {Coupling can be unstable in early phases}

end if

ALGORITHM 2. Algorithm to calculate the next step in the Hugoniot predictor for general polynomial and linear predictors. Other fitted forms could easily be used.

Input: P_{target} , history, V_0 , compression_in
Output: compression, derivative
steps taken = steps taken + 1
if steps taken > $2 \times$ steps requested **then**
 abort Too many steps taken {Avoid infinite runs}
end if
ndata = **min** (steps taken, history length)
if polynomial **and** steps taken > poly order + 1 **then**
 coeffs = polynomial_regression(history[1:ndata][ϵ], history[1:ndata][P], poly order) { $a + bx + cx^2 \dots$ }
 compression = solve_poly(P_{target} , coeffs)
 return $\max\left(\frac{-b \pm \sqrt{b^2 - 4c(a - P_{target})}}{2c}\right)$ {If poly order = 2 (i.e. quadratic)}
 derivative = -poly_deriv(compression) {Negative because compressing not expanding}
 return $2c \cdot \text{compression} + b$
Else
 coeffs = polynomial_regression(history[1:2][ϵ], history[1:2][P], 1) { $a + bx$ }
 derivative = $-b$
 compression = compression - $\left(\frac{P_{target} - P}{a}\right)$
end if
if |compression - compression_in| > max_comp_step **then**
 compression = compression_in + max_comp_step \times sgn(compression - compression_in)
end if

introduced a number of improvements to the original Hugoniot method that significantly improve the convergence rate of the calculation, and reduce the fluctuations, making it possible to achieve satisfactory ensemble averages without requiring very long runs and/or large numbers of atoms, so that now these methods can be used with *ab initio* methods instead of model potentials. This brings significant benefits in being able to calculate the Hugoniot of many materials. The results are in good agreement with available experimental data for some simple test systems.

The static compression of the constant-volume Hugoniot is much more amenable to *ab initio* simulations (especially those using a plane-wave basis) and as the cell properties are known from the start of the calculation it is also possible to account for the compression in the convergence of systematic parameters.

We have illustrated the performance and accuracy of our new approach by comparing it to the reference implementation of the Hugoniot in the LAMMPS code, for two different model potentials—Lennard-Jones (for argon) and BKS (with short-range corrections) for quartz. We also find that our extensions to the Hugoniot have significantly improved the equilibration times compared to those of LAMMPS without detracting from its accuracy. We have illustrated the effectiveness of the method by calculating the Hugoniot of argon using DFT, and show remarkable agreement to experiment, with no fitting parameters, for a system with only 108 atoms.

We have also introduced improvements to the coupling constants, which make it simple for a non-expert user to utilize. The advantage given by independence from requiring accurate couplings

for convergence is that the recommended estimates for optimal coupling given in Ravelo *et al.*¹⁷ are expensive to calculate, especially in an *ab initio* calculation. Not only that but they should be updated for different compressions to achieve rapid equilibration, which becomes prohibitive in an *ab initio* context.

Finally, the predictor method makes it simple for a complete Hugoniot curve to be generated in a single run, enabling optimal data reuse between different state points and minimizing transients caused by changes in compression. This is again very beneficial in *ab initio* calculations (Algorithm 1).

The ability to generate a Hugoniot automatically from a starting state for any material, in principle, gives great power to those who wish to be able to “black box” *ab initio* simulation and opens a new, wide range of properties to materials databasing projects. Given how important shock resilience is to a large number of engineering and geophysical sciences, this will doubtlessly prove essential in the future.

ACKNOWLEDGMENTS

We are grateful for computational support from the UK National High Performance Computing service, ARCHER/ARCHER2, for which access was obtained via the UKCP consortium and funded by EPSRC (Grant No. EP/P022561/1). Additional computational resources were provided by the University of York with the Viking Cluster, which is a high-performance computing facility supported by the University of York HPC service.

AUTHOR DECLARATIONS

Conflict of Interest

The authors have no conflicts to disclose.

Author Contributions

All authors co-wrote the paper. J.S.W. developed the algorithms and wrote the additional code. M.I.J.P. wrote the original MD code and conceived and designed the study.

Jacob S. Wilkins: Formal analysis (lead); Software (equal); Writing – original draft (equal); Writing – review & editing (equal).
Matt I. J. Probert: Conceptualization (lead); Software (equal); Supervision (lead); Writing – original draft (equal); Writing – review & editing (equal).

DATA AVAILABILITY

Example CASTEP input files used during the current study are available from <https://doi.org/10.15124/d291a266-2b4d-4528-a701-034e655bbcbe>.

APPENDIX: ALGORITHMS

Algorithm 1 is the Hugoniot predictor algorithm, with fail-safe, reuse, and Nosé–Hoover coupling sections. Algorithm 2 is the algorithm to calculate the next step in the Hugoniot predictor for general polynomial and linear predictors.

REFERENCES

- 1 E. F. Medici, J. S. Allen, and G. P. Waite, “Modeling shock waves generated by explosive volcanic eruptions,” *Geophys. Res. Lett.* **41**, 414–421, <https://doi.org/10.1002/2013gl058340> (2014).
- 2 D. Castelvetti, “Nature retracts controversial superconductivity paper by embattled physicist,” *Nature*, <https://www.nature.com/articles/d41586-023-03398-4> (2023).
- 3 M. Mareschal, S. McNamara, J.-B. Maillet, and R. Soto, “Non-equilibrium molecular dynamics simulations: Techniques and applications,” *AIP Conf. Proc.* **574**, 155–191 (2001).
- 4 S. Bernard and J. B. Maillet, “First-principles calculation of the melting curve and Hugoniot of tin,” *Phys. Rev. B* **66**, 012103 (2002).
- 5 J. Chang, P. Lian, D.-Q. Wei, X.-R. Chen, Q.-M. Zhang, and Z.-Z. Gong, “Thermal decomposition of the solid phase of nitromethane: *Ab initio* molecular dynamics simulations *ab initio* molecular dynamics simulations,” *Phys. Rev. Lett.* **105**, 188302 (2010).
- 6 T. K. Stenczel, Z. El-Machachi, G. Liepuoniute, J. D. Morrow, A. P. Bartók, M. I. J. Probert, G. Csányi, and V. L. Deringer, “Machine-learned acceleration for molecular dynamics in castep,” *J. Chem. Phys.* **159**, 044803 (2023).
- 7 B. W. Hamilton, M. N. Sakano, C. Li, and A. Strachan, “Chemistry under shock conditions,” *Annu. Rev. Mater. Res.* **51**, 101–130 (2021).
- 8 W. J. M. Rankine, “On the thermodynamic theory of waves of finite longitudinal disturbances,” *Philos. Trans. R. Soc. London* **160**, 277–288 (1870).
- 9 H. Hugoniot, “Mémoire sur la propagation des mouvements dans les corps et spécialement dans les gaz parfaits (première partie) [memoir on the propagation of movements in bodies, especially perfect gases (first part)],” *J. Ec. Polytech.* **57**, 3–97 (1887).
- 10 J.-B. Maillet, M. Mareschal, L. Souillard, R. Ravelo, P. S. Lomdahl, T. C. Germann, and B. L. Holian, “Uniaxial Hugoniot: A method for atomistic simulations of shocked materials,” *Phys. Rev. E* **63**, 016121 (2000).
- 11 E. J. Reed, L. E. Fried, and J. D. Joannopoulos, “A method for tractable dynamical studies of single and double shock compression,” *Phys. Rev. Lett.* **90**, 235503 (2003).
- 12 A. V. Kudinov, S. A. Gubin, and Y. A. Bogdanova, “Comparison of molecular dynamics simulation methods of methane shockwave compression,” *J. Phys.: Conf. Ser.* **1686**, 012081 (2020).
- 13 S. Plimpton, “Fast parallel algorithms for short-range molecular dynamics,” *J. Comput. Phys.* **117**, 1–19 (1995).
- 14 S. J. Clark, M. D. Segall, C. J. Pickard, P. J. Hasnip, M. I. J. K. M. C. ProbertRefsonPayne, K. Refson, and M. C. Payne, “First principles methods using CASTEP,” *Z. Kristallogr.—Cryst. Mater.* **220**, 567–570 (2005).
- 15 L. Rayleigh, “Aerial plane waves of finite amplitude,” *Proc. R. Soc. London, Ser. A* **84**, 247–284 (1910).
- 16 G. I. Kanel, V. E. Fortov, and S. V. Razorenov, *Shock-Wave Phenomena and the Properties of Condensed Matter* (Springer, New York, 2004), pp. 29–82.
- 17 R. Ravelo, B. L. Holian, T. C. Germann, and P. S. Lomdahl, “Constant-stress Hugoniot method for following the dynamical evolution of shocked matter,” *Phys. Rev. B* **70**, 014103 (2004).
- 18 P. Langevin, “Sur la théorie du mouvement Brownien [On the theory of Brownian motion],” *C. R. Acad. Sci.* **146**, 530–533 (1908) [*Am. J. Phys.* **65**, 1079–1081 (1997)].
- 19 B. Leimkuhler, E. Noorizadeh, and F. Theil, “A gentle stochastic thermostat for molecular dynamics,” *J. Stat. Phys.* **135**, 261–277 (2009).
- 20 J.-B. Maillet and G. Stoltz, “Sampling constraints in average: The example of Hugoniot curves,” *Appl. Math. Res. Express* **2008**, abn004.
- 21 D. Quigley and M. I. J. Probert, “Langevin dynamics in constant pressure extended systems,” *J. Chem. Phys.* **120**, 11432–11441 (2004).
- 22 M. I. J. Probert, “Improved algorithm for geometry optimisation using damped molecular dynamics,” *J. Comput. Phys.* **191**, 130–146 (2003).
- 23 P. Debye, “Zur theorie der spezifischen wärmen,” *Ann. Phys.* **344**, 789–839 (1912).
- 24 J. E. Lennard-Jones, “On the determination of molecular fields,” *Proc. R. Soc. London, Ser. A* **106**, 463–477 (1924).
- 25 B. W. H. van Beest, G. J. Kramer, and R. A. van Santen, “Force fields for silicas and aluminophosphates based on *ab initio* calculations,” *Phys. Rev. Lett.* **64**, 1955–1958 (1990).
- 26 R. A. Buckingham, “The classical equation of state of gaseous helium, neon and argon,” *Proc. R. Soc. London, Ser. A* **168**, 264–283 (1938).
- 27 M. R. Farrow and M. I. J. Probert, “Atomistic molecular dynamics simulations of shock compressed quartz,” *J. Chem. Phys.* **135**, 044508 (2011).
- 28 S. P. Marsh, *LASL Shock Hugoniot Data* (University of California Press, Berkeley, 1980), p. 324.
- 29 J. Wackerle, “Shock-wave compression of quartz,” *J. Appl. Phys.* **33**, 922–937 (1962).
- 30 I. Saika-Voivod, F. Sciortino, T. Grande, and P. H. Poole, “Phase diagram of silica from computer simulation,” *Phys. Rev. E* **70**, 061507 (2004).
- 31 M. Farrow, “Computer simulation of shock waves in condensed matter,” Ph.D. thesis (University of York, York, 2009).
- 32 R. D. Dick, R. H. Warnes, and J. Skalyo, “Shock compression of solid argon,” *J. Chem. Phys.* **53**, 1648–1651 (1970).
- 33 H. R. Moeller and C. F. Squire, “Ultrasonic velocities in solid argon,” *Phys. Rev.* **151**, 689–693 (1966).